J. Min. Metall. Sect. B-Metall. 50 (2) B (2014) 145 - 148

Journal of Mining and Metallurgy, Section B: Metallurgy

THERMODYNAMIC PROPERTIES OF THE LIQUID Ag-Bi-Cu-Sn LEAD-FREE SOLDER ALLOYS

G. Garzel, M.Kopyto, L. A. Zabdyr

Institute of Metallurgy and Materials Science, Polish Academy of Sciences, Laboratory of Physical Chemistry of Materials, Krakow, Poland

(Received 27 July 2013; accepted 02 April 2014)

Abstract

The electromotive force measurement method was employed to determine the thermodynamic properties of liquid Ag-Bi-Cu-Sn alloys using solid electrolyte galvanic cells as shown below:
Kanthal+Re, Ag-Bi-Cu-Sn, SnO_2 | Yttria Stabilized Zirconia | air, Pt,
Experiments were made within temperature interval: 950 – 1300K along four composition paths of constant ratios: $X_{Ag} : X_{Bi} : X_{Cu} = 1$, $X_{Ag} : (X_{Bi} + X_{Cu}) = 3:2$ for $X_{Bi} = X_{Cu}$, $X_{Bi} : (X_{Ag} + X_{Cu}) = 3:2$ for $X_{Ag} = X_{Cu}$ and $X_{Cu} : (X_{Ag} + X_{Bi}) = 3:2$ for $X_{Ag} = X_{Bi}$ and tin concentration changing from 0.1 to 0.9 mole fractions, every 0.1. Almost all the results were approximated by straight line equations: EMF vs T, and tin activities were then calculated in arbitrary temperature; measurement results were presented by graphs. Unusual activity plot for $X_{Bi} : (X_{Ag} + X_{Cu}) = 3:2$ composition path was most probably caused by miscibility gap detected earlier in Bi-Cu-Sn ternary liquid alloys.

Keywords: Electrochemical techniques, Thermodynamic properties, Lead-free solders.

1. Introduction

Over the past years attention, was paid to the determination of thermodynamics and phase equilibria in systems based on silver, bismuth, copper and tin. Alloys based on those components are considered among others as possible materials for the lead-free solders [1-5]. Systematic experimental and theoretical studies of thermodynamic properties [e.g.,6-14] , made by the various research centers partially coordinated by the European actions COST531 [15] and MP609 [16] led to the development of complete thermodynamics descriptions of the binary and ternary systems based on those elements [e.g.,17-21]. Phase boundaries and chemical composition of quaternary Ag-Bi-Cu-Sn system were investigated by Doi at all [22] using differential scanning calorimetry (DSC), optical microscope and a scanning electronic microscope (TEM) while the chemical compositions were determined by energy dispersive X-ray microanalyzer (EDX). The detailed knowledge of the phase equilibria in this quaternary system is essential for at least two reasons one to make an efficient alloy design easier and the second to understand and predict the interactions in different conditions between Ag-Bi-Sn solder and copper, which is frequently used as substrate in the electronics industry.

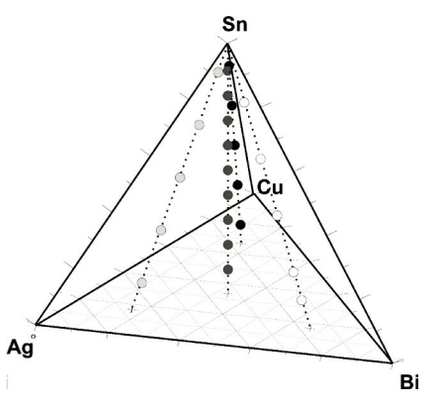

Figure 1. *Measured alloy compositions in quaternary Ag-Bi–Cu–Sn.*

2. Experimental

Details of both experimental equipment and procedure were described in our earlier paper [6,9,10].

Silver-bismuth-copper-tin alloys were prepared from pure metals (Ag, Bi and Sn 99.99%, Cu 99.999%) by direct melting in the electrolyte tube with SnO_2 (99.99%) pellet. Sample compositions were changed along four paths of constant ration: $X_{Ag} : X_{Bi} : X_{Cu} = 1$, $X_{Ag} : (X_{Bi} + X_{Cu}) = 3:2$ for $X_{Bi} = X_{Cu}$, $X_{Bi} : (X_{Ag} + X_{Cu}) = 3:2$ for $X_{Ag} = X_{Cu}$ and $X_{Cu} : (X_{Ag} +$

* *Corresponding author: g.garzel@imim.pl*

DOI:10.2298/JMMB130727015G

X_{Bi}) = 3:2 for $X_{Ag} = X_{Bi}$ and tin concentration changing from 0.1 to 0.9 mole fractions, every 0.1, Fig.1, resulting in 24 different alloy compositions. Control of composition samples was made by EDS at least once for each path.

An inert atmosphere was maintained inside the cell by passing 5 ml/min argon gas of quality 5.0 (Linde, Poland) through the H-tube. Passing gas through the H-tube allowed a penetration by inert gas into the electrolyte tube without disturbing the local equilibrium over the sample.

The reversibility of the cell was checked by passing small current from an external source; the e.m.f. returned to the original value within ±1mV in about 1-10 min depending on the temperature. The e.m.f. readings were taken in both heating and cooling mode within the range 950-1300K producing almost the same e.m.f. values within recorded scatter of points. The full run was completed after about 3-4 days.

3. Results

In order to determine tin activities in liquid Ag-Bi-Cu-Sn alloys the e.m.f. of the cell (I):

Kanthal+Re, Ag-Bi-Cu-Sn, SnO_2 | Yttria Stabilized Zirconia | air, Pt, $P_{O_2} = 0.21\ atm$ (I)

was measured in the temperature range and alloy compositions mentioned above.

During the work of the cell the following reaction take place:

a) at reference electrode:

$$O_2(g) + 4e^- = 2[O^{-2}] \quad (1)$$

b) at alloy electrode:

$$\underline{Sn(l)} + 2[O^{-2}] = 4e^- + SnO_2(s) \quad (2)$$

where $\underline{Sn(l)}$, e^-, $O_2(g)$ and $[O^{-2}]$ denote: tin in a metallic liquid solution, electron, pure oxygen gas and oxygen ion, respectively.

Consequently, the overall cell (I) reaction is:

$$\underline{Sn(l)} + O_2(g) = SnO_2(s) \quad (3)$$

For the reversible reaction (3) the change in Gibbs free energy can be derived as follows:

$$\Delta G(3) = -4FE = \Delta G^0_{f,SnO_2} - RT \ln a_{Sn} - RT \ln(0.21) \quad (4)$$

If tin is in its pure, liquid state (X_{Sn} = 1) equation (4) takes the form:

$$\Delta G^0_{f,SnO_2} = -4FE^0 + RT \ln(0.21) \quad (5)$$

Then, from equation (5) the Gibbs energy of formation of the solid SnO_2, for reaction $Sn(l)+O_2(g) = SnO_2(s)$, can be determined from measured as a function of temperature. Next, by combining equations (4) and (5) the following expression for the activity of tin in the Ag-Bi-Cu-Sn liquid alloy can be derived, as below:

$$\ln a_{Sn} = \frac{4F}{RT}(E - E^0) \quad (6)$$

where F is the Faraday constant, T is the absolute temperature, and R is the gas constant.

All emf values were corrected for Pt-Kanthal thermoelectric power derived in the separate experiments: Ep= -0.236363-5.45794 $\cdot 10^{-4}T$+8.31592 $\cdot 10^{-6}T^2$ [mV]. Rhenium tip was small enough to fit the constant temperature zone, so the respective thermoelectric correction was not taken into consideration.

The results of temperature dependence of e.m.f. E^0 obtained for pure tin were determined in one of our previous works [10]; they can be presented in the form:

$$E^0(V) = 1.478\ (\pm 0.002) - 0.5553\ (\pm 0.0013) \cdot T \quad (7)$$

Combining (5) and (7), the Gibbs free energy of formation of solid SnO_2 in reaction:

$$Sn(l) + O_2(g) = SnO_2(s) \quad (8)$$

from liquid tin and gaseous oxygen is given by the expression:

$$\Delta G^0_{f,SnO_2},\ kJ/mol = -\mathbf{570.4}(\pm 0.6) + \mathbf{0.2013}(\pm 0.0046) \cdot T \quad (9)$$

Linear dependence of e.m.f. on temperature was observed for all alloy compositions and parameters of equations: $E = a + b \cdot T$ obtained by the least square fit of e.m.f. data are listed for all measured cross section in Tables 1 – 4; and the example of the *e.m.f.* versus T plot for the path $X_{Ag} : X_{Bi} : X_{Cu} = 1$ is shown in Figure 2.

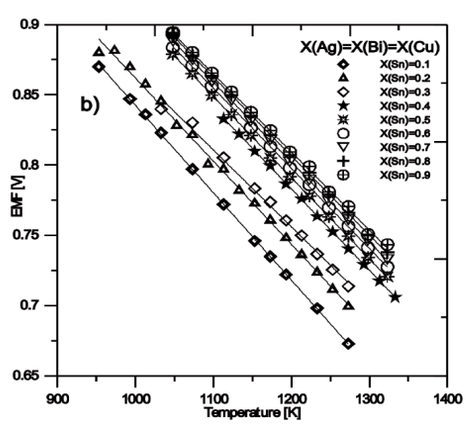

Figure 2. *E.m.f vs. temperature plots for cross-section $X_{Ag} : X_{Bi} : X_{Cu} = 1$*

Since the statistical scatter of the *e.m.f* vs *T* plots is very small it was assumed that e.m.f values calculated via linear equations of Tables 1 - 4 are equal to those measured within an experimental error, relation (6) was used to derive activity data at the arbitrary temperature 1273K; plots of tin activity vs tin content for composition path order mentioned above are presented in Figure 3.

Table 1. *Corrected e.m.f. versus temperature line coefficients for different tin concentration in Ag-Bi-Cu-Sn liquid alloys for cross-section X(Ag)/[X(Bi)+X(Cu)]=3/2.*

X_{Sn}	$E= a(\pm\Delta a)+ b(\pm\Delta b)\cdot T, V$			
	$a(\pm\Delta a)$		$b(\pm\Delta b)$	
0.1	1.4450	(±0.0174)	-6.05E-04	(±0.14E-04)
0.3	1.4918	(±0.0168)	-6.03E-04	(±0.14E-04)
0.5	1.4953	(±0.0231)	-5.87E-04	(±0.19E-04)
0.7	1.4907	(±0.0156)	-5.73E-04	(±0.13E-04)
0.9	1.4784	(±0.0215)	-5.59E-04	(±0.18E-04)

Table 2. *Corrected e.m.f. versus temperature line coefficients for different tin concentration in Ag-Bi-Cu-Sn liquid alloys for cross-section X(Bi)/[X(Ag)+X(Cu)]=3/2*

X_{Sn}	$E= a(\pm\Delta a)+ b(\pm\Delta b)\cdot T, V$			
	$a(\pm\Delta a)$		$b(\pm\Delta b)$	
0.1	1.3433	(±0.0274)	-4.87E-04	(±0.25E-04)
0.2	1.4330	(±0.0088)	-5.56E-04	(±0.07E-04)
0.4	1.3908	(±0.0151)	-4.95E-04	(±0.12E-04)
0.6	1.3696	(±0.0300)	-4.69E-04	(±0.25E-04)
0.8	1.4538	(±0.0580)	-5.43E-04	(±0.48E-04)

Table 3. *Corrected e.m.f. versus temperature line coefficients for different tin concentration in Ag-Bi-Cu-Sn liquid alloys for cross-section X(Cu)/[X(Ag)+X(Bi)]=3/2.*

X_{Sn}	$E= a(\pm\Delta a)+ b(\pm\Delta b)\cdot T, V$			
	$a(\pm\Delta a)$		$b(\pm\Delta b)$	
0.1	1.3447	(±0.0185)	-5.24E-04	(±0.15E-04)
0.3	1.4588	(±0.0036)	-5.78E-04	(±0.03E-04)
0.5	1.4965	(±0.0080)	-5.88E-04	(±0.06E-04)
0.7	1.4693	(±0.0200)	-5.59E-04	(±0.16E-04)
0.9	1.4812	(±0.0136)	-5.61E-04	(±0.11E-04)

Table 4. *Corrected e.m.f. versus temperature line coefficients for different tin concentration in Ag-Bi-Cu-Sn liquid alloys for cross-section X(Ag)=X(Bi)=X(Cu)*

X_{Sn}		$E= a(\pm\Delta a)+ b(\pm\Delta b)\cdot T, V$		
		$a(\pm\Delta a)$	$b(\pm\Delta b)$	
0.1	1.4645	(±0.0033)	-6.22E-04	(±0.03E-04)
0.2	1.4536	(±0.0103)	-5.92E-04	(±0.09E-04)
0.3	1.4119	(±0.0179)	-5.47E-04	(±0.15E-04)
0.4	1.4777	(±0.0023)	-5.79E-04	(±0.01E-04)
0.5	1.4842	(±0.0023)	-5.78E-04	(±0.02E-04)
0.6	1.4828	(±0.0030)	-5.71E-04	(±0.02E-04)
0.7	1.4834	(±0.0024)	-5.68E-04	(±0.02E-04)
0.8	1.4821	(±0.0026)	-5.63E-04	(±0.02E-04)
0.9	1.4767	(±0.0076)	-5.56E-04	(±0.06E-04)

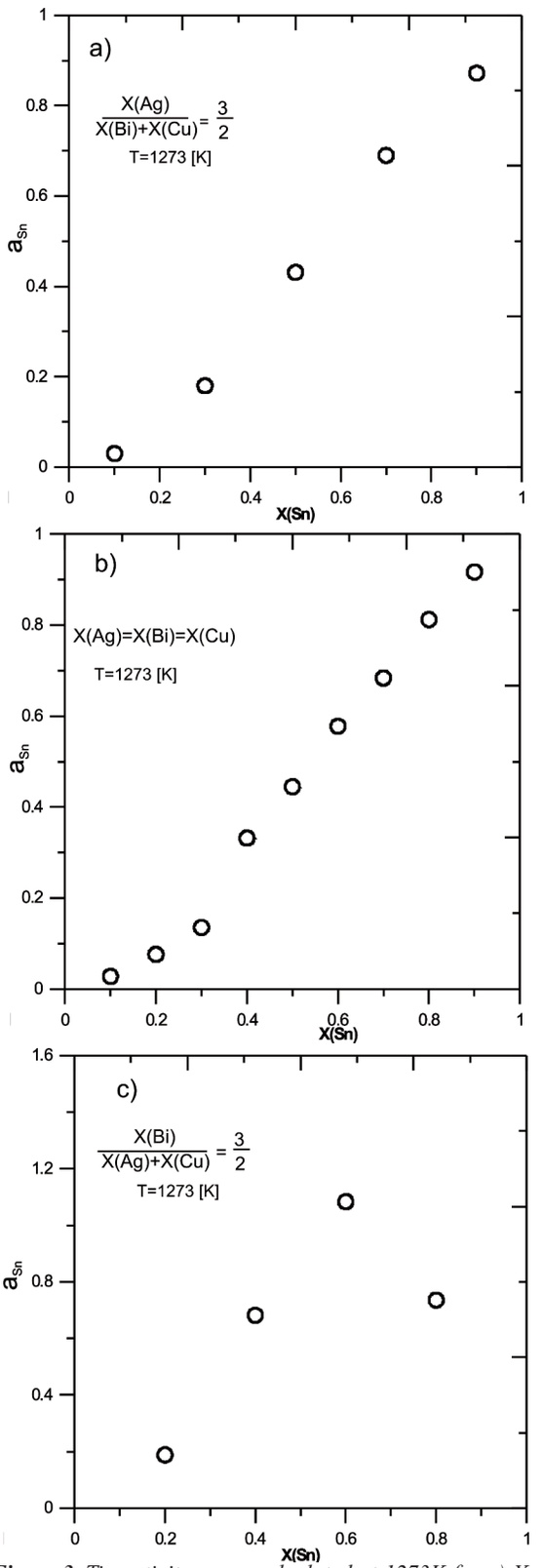

Figure 3. *Tin activity curve calculated at 1273K for a) $X_{Ag} : (X_{Bi} + X_{Cu}) = 3:2$ b) $X_{Ag} : X_{Bi} : X_{Cu} = 1$ c) $X_{Bi} : (X_{Ag} + X_{Cu}) = 3:2$*

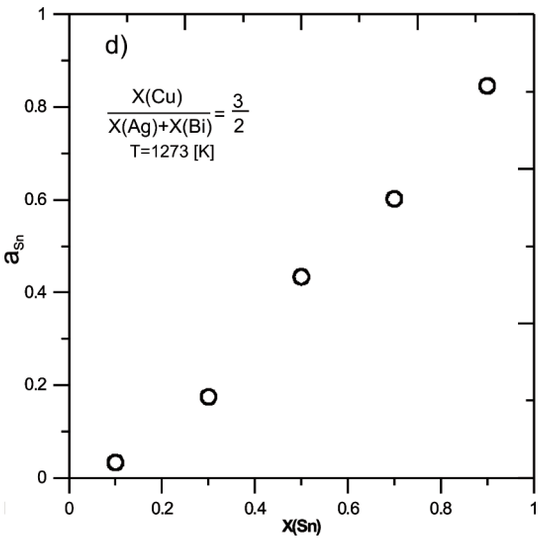

Figure 3. *Tin activity curve calculated at 1273K for d) X_{Cu} : (X_{Ag} + X_{Bi}) = 3:2*

5. Conclusions

Tin activities in the liquid Ag-Bi-Cu-Sn alloys were determined for the first time by emf method using solid electrolyte galvanic cells. Linear dependence of emf on temperature was observed in all 24 compositions investigated.

Activity versus composition plots as shown in Fig. 3 displays slightly negative deviation from Raoult's rule for lower tin contents, whereas for higher ones deviation is slightly posiive. Unusual activity plot for X_{Bi} : (X_{Ag} +X_{Cu}) = 3:2 composition path was most probably caused by miscibility detected in Bi-Cu-Sn ternary liquid alloys [22].

Aknowledgement

This study was performed within the frame of European program "COST Action MP0602 – Hisold". The financial support from Polish Ministry of Science and Higher Education under grant No 85/N-COST/2007/0 has been gratefully aknowledged.

References

[1] I. Ohnuma, M. Miyashita, K. Anzai, X.J. Liu, H. Ohtani, R. Kainuma, K. Ishida. Journal of Electronic Materials, 29 (10) (2000) 1137-1144.

[2] J.-M. Song, H.-Y. Chuang, Z.-M Wu. Journal of Electronic Materials, 35 (5) (2006) 1041-1049.

[3] J.-M. Song, H.-Y. Chuang, Z.-M Wu. Journal of Electronic Materials, 36 (11) (2007) 1516-1523.

[4] Y. Takamatsu, H. Esaka, K. Shinozuka, Nippon Kinzoku Gakkaishi/Journal of the Japan Institute of Metals, 74 (2) (2010) 101-109.

[5] I. Ohnuma, R. Kainuma, K Ishida. Journal of Mining and Metallurgy, Section B: Metallurgy, 48 (3) (2012) 413-418.

[6] G. Garzeł, L.A. Zabdyr, Journal of Phase Equilibria and Diffusion, 27 (2) (2006) 140-144.

[7] H. Flandorfer, A. Sabbar, C. Luef, M. Rechchach, H. Ipser, Thermochimica Acta, 472 (1-2) (2008) 1-10.

[8] Z. Li, Z. Cao, S. Knott, A. Mikula, , Y. Du, Z. Qiao, Calphad: Computer Coupling of Phase Diagrams and Thermochemistry, 32 (1) (2008) 152-163.

[9] M. Kopyto, G. Garzel, L.A. Zabdyr, Journal of Mining and Metallurgy, Section B: Metallurgy, 45 (1) (2009) 95-100.

[10] M. Kopyto, B. Onderka, L.A. Zabdyr, Materials Chemistry and Physics, 122 (2-3) (2010) 480-484.

[11] J. Romanowska Archives of Metallurgy and Materials, 56 (1) (2011) 87-91.

[12] D. Živković, D. Minić, D. Manasijević, N. Talijan, I. Katayama, , A. Kostov Journal of Materials Science: Materials in Electronics, 22 (8) (2011) 1130-1135.

[13] Z. Guo, W. Yuan, M. Hindler, A. Mikula. Journal of Chemical Thermodynamics, 48 (2012) 201-206.

[14] P. Fima, G. Garzel, Calphad: Computer Coupling of Phase Diagrams and Thermochemistry, 44 (2014) 48-53.

[15] A. Kroupa, A.T. Dinsdale, A. Watson, J. Vrestal, A. Zemanova, Journal of Mining and Metallurgy, Section B: Metallurgy, 43 (2) (2007) 113-123.

[16] A. Kroupa, A. Dinsdaleb, A. Watsonc, J.J. Vřešťál, A. Zemanova, P. Broz, Journal of Mining and Metallurgy, Section B: Metallurgy, 48 (3) (2012) 339-346.

[17] L.A. Zabdyr, G. Garzeł, Calphad: Computer Coupling of Phase Diagrams and Thermochemistry, 33 (1) (2009) 187-191.

[18] H. Ipser, H. Flandorfet, Ch. Luef, C. Schmetterer, U. Saeed. Journal of Materials Science: Materials in Electronics, 18 (1-3) (2007)3-17.

[19] A. Dinsdale, A. Watson, A. Kroupa, J. Vrestal, A. Zemanowa, J. Vizdal, COST Action 531 - Atlas of phase diagrams for lead-free soldering (2008).

[20] SOLDERS Database for Lead Free Solders (2008).

[21] K. Doi, , H. Ohtani, , M. Hasebe, Materials Transactions, 45 (2) (2004) 380-383.

[22] B. Ma, J. Li, Z. Peng, G. Zhang, Journal of Alloys and Compounds, 535 (2012) 95-101.